Exploring Gap Junctions Locations and Density in a Network of Model Neurons with Resonant Dendrites

Davide Michieletto, Dr Yulia Timofeeva

University of Warwick, Complexity Centre, Zeeman Building
(Dated: June 11, 2012)

Abstract. Dendrites are one of the central research topics in neuroscience. They show fascinating complex geometries, non-linear voltage dynamics and countless synaptic connections. Dendritic morphology and intrinsic resonant properties are two of the main features that should be taken into account when we want to model real networks of neurons. Moreover, gap-junctions have been shown to play an important role of tuning network dynamics of spatially extended neurons. In this project we aim to investigate, at the single cell level, how the dynamical properties of the dendritic membranes affect the generation of spikes in the soma, as a function of the dendritic natural frequency and coupling strength between somatic and dendritic compartments. At the network level, we are interested to explore how location and strength of gap-junctions control the response function of a network. To get some mathematical insight, we consider a network of two spatially extended quasi-active neurons connected by a gap-junction and analytically construct the Green's function $G_{ij}(x, y, w)$.

I. INTRODUCTION

Dendrites cover a major role in brain activity and signal processing. Many experiments[1–5] have shown that the responses of certain regions of the brain to electrical stimuli are frequency dependent, namely, dendrites do not behave only as passive cables, but they have an actual crucial role in filtering and processing the electrical signals. The activity of the dendritic membranes makes them quite difficult to describe analytically, but at the same time, gives rise to complex and fascinating band-pass features. Mauro *et al.*[6] have suggested a linearised model that extends the more usual 'RC' circuit description for passive membranes to a 'RLC' circuit description for the linearised dynamics of active membranes, to which is often referred as model for quasi-active membranes. Activity is not the only problem arising when one tries to describe dendritic behaviour. In fact, dendrites show also very complex geometries and developed branched structures. Koch and Poggio[7] have shown how to numerically compute response functions of the dendritic voltage in the Laplace (frequency) domain for arbitrary linearised membranes. Abbott *et al.*[8] applied the path integral formalism to analytically compute the Green's functions (response functions) $G_{ij}(x, y, t)$ for any branched passive dendritic tree in time domain between two points x and y in two different branches i and j. Recently, Coombes *et al.*[9] generalised the works by Koch and Abbott, showing that the path integral formalism can be extended to quasi-active membranes but must be modified to take into account resonant properties of the membranes. Finally, dendrites not only have non-linear dynamics and complex spatial configurations but they even are connected to each other. In particular, electrical synapses, or gap-junctions, are abundant in the brain and are believed to affect normal and abnormal physiological brain rhythms, including epilepsy. As recently shown numerically[10], gap-junctions can indeed strongly affect the synchronization of connected neurons and are, therefore, a crucial element to be considered whenever a network of spatially extended neurons is modelled.

Using what has already been done on the different aspects mentioned above, we aim to unify all the major results under a unique framework and describe the behaviour of networks of spatially extended quasi-active neurons connected by gap-junctions. In section **II** we give a brief mathematical introduction on the linearisation of active membranes and how they can be modelled through simple 'RLC' circuits. In section **III** we introduce a basic non-spatial model in

which an active soma and a quasi-active dendrite are coupled in a two-compartmental model. In the same section we focus on filtering properties and mutual feedback between soma and dendrite. Section **IV** includes a more realistic spatially extended model. According to Koch[11] we show how the band-pass properties of long quasi-active cables can explain biologically observed phenomena as the differentiation of morphology of ganglion cells in the retina[4]. Finally, section **V** is focused on the derivation of an analytical compact form for the Green's function in the case of a small network of neurons joined by a gap-junction. The analytical form in the Laplace domain will then be validated numerically by brute force numerical simulations and it will give an insight into an analytical formulation of the contribution of gap-junction connection to the voltage dynamics into the network. In section **VI** we provide some discussion of the further potential of this work.

II. QUASI-ACTIVE MEMBRANES

In this section we briefly recall the linearisation of active membranes suggested by Mauro *et al.*[6]. Active dendrites can be linearised about their resting state, and they still display realistic resonant behaviour for small enough deviation of the voltage from the resting value. This linearisation leads to the so called 'quasi-active' membranes, which have been successfully described by 'RLC' circuits, instead of the most common 'RC' circuits for the passive membranes. Below we briefly review the linearisation procedure and show how the linearised model may be described in the language of 'RLC' circuits. We consider a generic active ionic membrane current of the form

$$I = I(V, w),$$

where V is the voltage and w is the gating variable (we restrict ourselves to the case of only one gating variable) that satisfies:

$$\tau(V)\dot{w} = w_\infty - w, \tag{1}$$

where it is traditional to write

$$\begin{aligned} \tau(V) &= (\alpha(V) + \beta(V))^{-1}, \\ w_\infty(V) &= \alpha(V)\tau(V). \end{aligned} \tag{2}$$

Now considering a small variation from the resting values $(V^*, w^*) = (V^*, w_\infty(V^*))$ we get

$$\delta I = \left.\frac{\partial I}{\partial V}\right|^* \delta V + \left.\frac{\partial I}{\partial w}\right|^* \delta w = g\delta V + \left.\frac{\partial I}{\partial w}\right|^* \delta w, \tag{3}$$

where $g = \partial I/\partial V|^*$ and the superscript $*$ denotes quantities which are evaluated at the resting state. Using the relations (2) we can write the evolution of the gating variable (1) as

$$\left[\frac{d}{dt} + (\alpha+\beta)|^*\right]\delta w = \left[\frac{d\alpha}{dV} - w_\infty \frac{d(\alpha+\beta)}{dV}\right]\Bigg|^* \delta V,$$

and therefore we may substitute the expression for δw in (3), obtaining

$$\delta I = g\delta V + \delta J, \tag{4}$$

with $\delta J = \partial I/\partial w|^* \delta w$ and for which it holds

$$\left[R + L\frac{d}{dt}\right]\delta J = \delta V, \tag{5}$$

with

$$r^{-1} = \tau^* \frac{\partial I}{\partial w}\left[\frac{d\alpha}{dV} - w_\infty \frac{d(\alpha+\beta)}{dV}\right]\Bigg|^*, \tag{6}$$

$$L = \tau^* R, \tag{7}$$

where $\tau^* = \tau(V^*)$.
The equations (4) and (5) tell us that for small deviations from the resting state, the (linearised) current I behaves like in a 'RLC' circuit where the leakage conductance g is in parallel with a branch with a resistance R and an inductance L in series.

III. TWO-COMPARTMENT MODEL

We first consider a system in which a quasi-active membrane is coupled to a soma whose activity is described by the Morris-Lecar model[12]. Both soma and dendrite are point-like and the strength of the coupling is parametrised by the conductance g_c (see fig.**1**). According to section **II**, the equations for the dynamics of the voltage in the dendritic compartment are:

$$\begin{aligned} C_d\frac{dV_d}{dt} &= -g_{L,d}(V_d - V_{L,d}) - I + g_c(V_s - V_d), \\ L\frac{dI}{dt} &= -RI + V_d, \end{aligned} \tag{8}$$

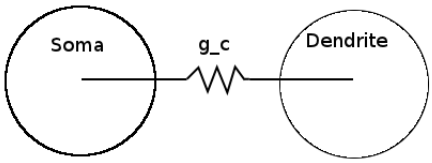

FIG. 1: Cartoon of the two compartments model showing somatic and dendritic compartments joined by the coupling g_c.

with $R_L^{-1} = g_{L,d}$ the leaky conductance, R the resistance and L the inductance through which we model the activity of the membrane. $V_{L,d}$ is the reversal potential of the dendrite (from now on set to 0). The voltage into the somatic compartment obeys the standard Morris-Lecar model plus the coupling term:

$$\begin{aligned} C\frac{dV_s}{dt} =& -g_L(V_s - V_L) - g_{Ca}m_\infty(V_s)(V_s - V_{Ca}) \\ & - g_K w(V_s)(V_s - V_K) + I_s + g_c(V_d - V_s), \\ \tau_w(V_s)\frac{dw}{dt} =& \, w_\infty(V_s) - w, \end{aligned} \tag{9}$$

with

$$\begin{aligned} m_\infty(V_s) &= \frac{1}{2}\left[1 + \tanh\frac{V_s - V_1}{V_2}\right], \\ w_\infty(V_s) &= \frac{1}{2}\left[1 + \tanh\frac{V_s - V_3}{V_4}\right], \\ \tau_w^{-1}(V_s) &= \phi\cosh\frac{V_s - V_3}{V_4}. \end{aligned}$$

In appendix **A** we report the values of the parameters used in the simulations. The dendritic parameters are, if not mentioned otherwise, fixed throughout the paper, and take values $C_d = 1\ \mu F$, $g_{L,d} = 0.05\ mS$ and $V_{L,d} = 0\ mV$.

A. Filtering Properties

In order to test the filtering behaviour of the quasi-active dendritic compartment we suppress the soma-dendrite coupling and inject a chirp stimulus in the dendritic compartment defined by:

$$I_{chirp}(t) = A\sin(w_{chirp}t^2) \tag{10}$$

with $w_{chirp} = 10^{-3}\ ms^{-2}$ and $A = 1\ \mu A$. The response to this stimulus shows two completely different behaviour for different values of R (see fig. **2**).

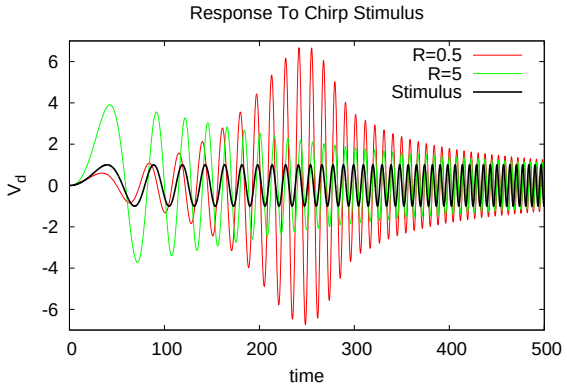

FIG. 2: Dendritic response $V_d[mV]$ to a periodic stimulus $I_{chirp}(t)$ injected into the dendritic compartment in case of zero coupling ($g_c = 0$) with the soma and for $R = 0.5\ k\Omega$ and $R = 5\ k\Omega$. The inductance is fixed to $L = 5\ kH$.

One can clearly notice a band pass behaviour for $R = 0.5\ k\Omega$ while a low-band pass (or passive) behaviour for higher R. In the next section we will see how this feature is justified by the complex impedance $Z(w; R, L)$.

1. *Impedance*

As one can notice in fig. **2**, the response for low R is peaked around a certain frequency $w^* = w_{chirp}t^*$, where t^* is the time at which the response takes the absolute maximum value. We have already mentioned that the system can be modelled by 'RLC' circuit. In this case the most useful function in order to study the frequency response of a circuit is the impedance $Z(w; R, L)$. Our membrane can be seen as made of a leaking branch with resistance $R_{L,d} = 1/g_{L,d}$ in parallel with a branch made of R and L in series. Therefore the total complex impedance can be expressed as

$$Z(w; R, L)^{-1} = R_{L,d}^{-1} + iwC_d + (R + iwL)^{-1}, \tag{11}$$

whose squared amplitude is

$$|Z(w; R, L)|^2 = \frac{R_{L,d}^2\left(R^2 + w^2L^2\right)}{\chi_1(L)w^4 + \chi_2(R, L)w^2 + \chi_3(R)}, \tag{12}$$

where

$$\chi_1(L) = (R_{L,d}C_dL)^2\,,$$
$$\chi_2(R,L) = L^2 + (C_dR_{L,d}R)^2 - 2C_dR_{L,d}^2L,$$
$$\chi_3(R) = (R+R_{L,d})^2\,.$$

Our goal is to find an analytical expression for w^* such that, for given R and L we know the exact value of the resonant frequency. In order to do that we simply maximise (12) with respect to w, which gives:

$$w^{*2}(R,L) = -\left(\frac{R}{L}\right)^2 + \left[\left(\frac{R}{L}\right)^4 - D(R,L)\right]^{1/2}, \tag{13}$$

where $D(R,L)$ is:

$$D(R,L) = \frac{\chi_2(R,L)R^2 - \chi_3(R)L^2}{\chi_1(L)L^2}. \tag{14}$$

In fig. **3** we show the surface $w^*(R,L)$. From this figure we can get numerical values of R and L for which w^* is constant. In particular the contours $w^* = const$ are shown in fig. **4**. Knowing the exact resonant frequency $w^*(R,L)$ for fixed R and L will be useful later on, when we will tune the firing frequency of the soma with the resonant frequency of the dendritic compartment.

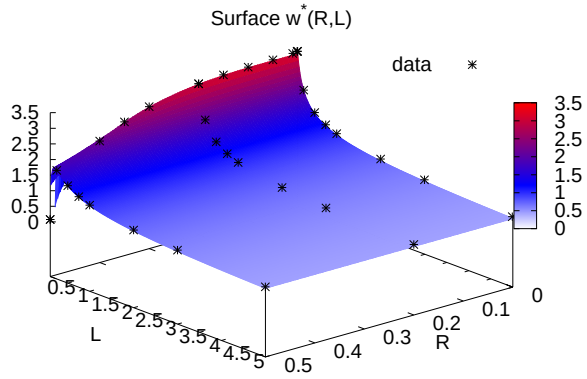

FIG. 3: Three dimensional plot of $w^*(R,L)$. Notice that the resonant frequency $w^* \to 0$ rapidly as R and L increase, showing a low-band pass, i.e. passive, behaviour. In particular the passive case is fully restored for $R \to \infty$ as the impedance becomes a monotonic decreasing function of the frequency.

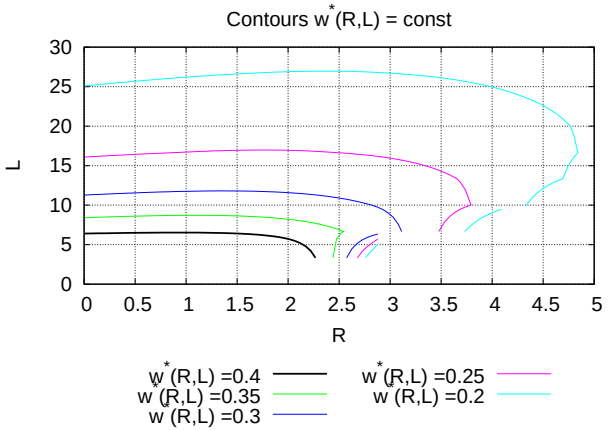

FIG. 4: Contours $w^*(R,L) = const\ [rad/ms]$. Contours are here used to choose the values for R and L in order to tune the dendritic resonant frequency with the firing frequency of the somatic compartment.

B. Role of Coupling Constant

Until now the coupling with the soma was suppressed. We now move to to the case $g_c \neq 0$. The equations (8) for the dendritic compartment can be therefore rearranged in the following way:

$$C_d\frac{dV_d}{dt} = -(g_{L,d}+g_c)V_d - I + g_cV_s,$$
$$L\frac{dI}{dt} = -RI + V_d. \tag{15}$$

From the first equation above one can notice that switching the coupling on, gives rise to an effective conductance $g' = g_{L,d} + g_c$ plus an injected current $I_{eff} = g_cV_s$. Therefore, it is easy to extend our calculation for $w^*(R,L)$ to the case in which $g_{L,d} \to g'$. A direct measurement of this ansatz can be quickly achieved varying the coupling parameter g_c and observing at which value w^*_{meas} the peak of the signal takes place. In fig. **5** we show the response of the dendrite to a chirp stimulus when it is coupled to the soma with $I_s = 0mV$, i.e. the soma is at its resting value $V_L = -60mV$.
A table with the predicted values of the peaks using the ansatz (15) and the observed ones is reported below. Measured values and predicted ones using g' are in perfect agreement.

Moreover it is worth noting that the average values of V_d in fig. **5** decrease as g_c increases.

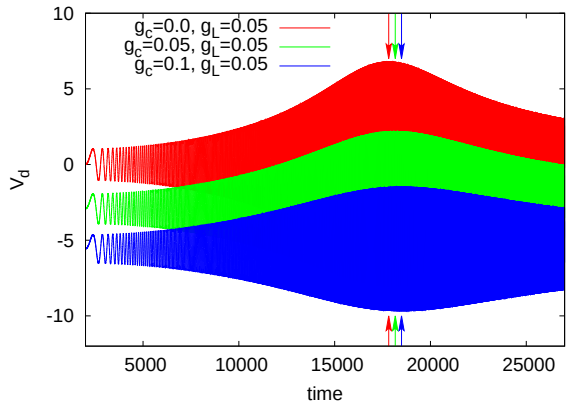

FIG. 5: Response of the dendrite when stimulated with a chirp stimulus in presence of coupling with soma. Here: $R = 1.1\ k\Omega$ and $L = 10.4\ kH$. In figure are plotted three different cases, i.e. $g_c = 0$, $g_c = 0.05$ and $g_c = 0.1\ mS$, with fixed $g_{L,d} = 0.05\ mS$. Arrows show when the maximum w^* appears.

$g_{L,d}$	g_c	g'	$w^*(g')$	$w^*(g_{L,d})$	w^*_{meas}
0.05	0.0	0.05	0.316	0.316	0.316
0.05	0.05	0.1	0.323	0.316	0.323
0.05	0.1	0.15	0.330	0.316	0.330

FIG. 6: Theoretical values for the natural frequencies $w^*(R, L; g')$ compared with the those computed using $w^*(R, L; g_{L,d})$ and the observed values from fig. **5** for fixed $R = 1\ k\Omega$ and $L = 10.4\ kH$.

This is due to the fact that the soma is at its resting value $V_s = -60\ mV$ and the stronger the coupling between soma and dendrite, the lower the dendritic resting value is, because of the effective current $g_c V_s$.

From the point of view of the soma, the introduction of the coupling term $I_c = g_c(V_d - V_s)$ is not without consequences on its unperturbed behaviour. In the following we study the effect of the coupling term on the Hopf bifurcations shown by the Morris-Lecar model. In particular we will track the lower Hopf bifurcation since if we keep the values of R and L in the range shown in fig. **4** then $w^* \sim 0.3\ rad/ms$ which correspond to oscillations with quite long period. In fig. **7** we show the position of the (lower) Hopf bifurcation on the (I_s, g_c) plane. As shown, the 'firing' (spontaneously oscillating) region of the somatic compartment shrinks as g_c grows, or in other words, for higher

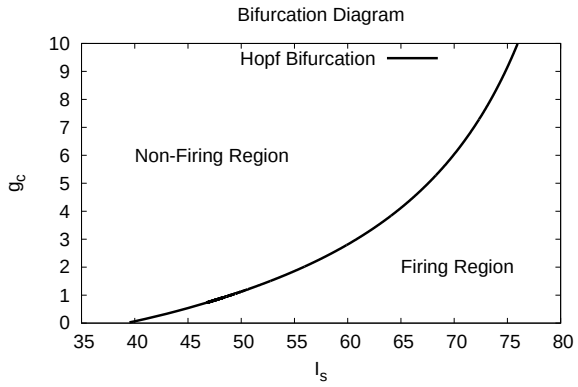

FIG. 7: Bifurcation diagram $(I_s\ [\mu A], g_c\ [mS])$ for $R = 1\ k\Omega$ and $L = 16.5512\ kH$. The line divides the regions where the soma shows a stable limit cycle (right) and one where it shows a stable fixed point (left). For small values of g_c the Hopf bifurcation merges with a limit point.

values of the coupling constant, the soma needs higher values of the current I_s in order to show a oscillating behaviour.
Notice that for small g_c, the Morris-Lecar model considered (see appendix **A**) shows a SNIC point (saddle-node on invariant cycle), where Hopf bifurcation and limit point merge. The extrapolated value of I_s at $g_c = 0$, which is $I_s(g_c = 0) = 39.6\ \mu A$, agrees with our simulations.

C. Mutual Feedback

In this section we study the effects of the mutual feedback between soma and dendrite, especially when they are in tune with each other . We have already seen that for certain values of the parameters R and L, the dendritic compartment shows a strong frequency dependent behaviour. Therefore, for fixed values of R and L, we expect that when the firing frequency of the soma (w_{soma}) is close to the dendritic natural frequency (w^*), the dendritic response will be boosted, and hence, the effect on the soma itself more visible. In the following we introduce a temporary parameter p which controls the direction of the current between soma and dendrite. For $p = 0$ the current flows

from the soma into the dendrite but not vice versa, while for $p = 0.5$ both current directions are allowed. In fig. **8** we show the somatic and dendritic voltage dynamics for $p = 0$ and $p = 0.5$ in the cases that $w_{soma} > w^*$ (top) and that $w_{soma} \sim w^*$ (bottom). The firing frequency of the soma w_{soma} has been directly measured for different I_s in the case of isolated soma. In appendix **C** report the values $w_{soma}(I_s)$ measured.

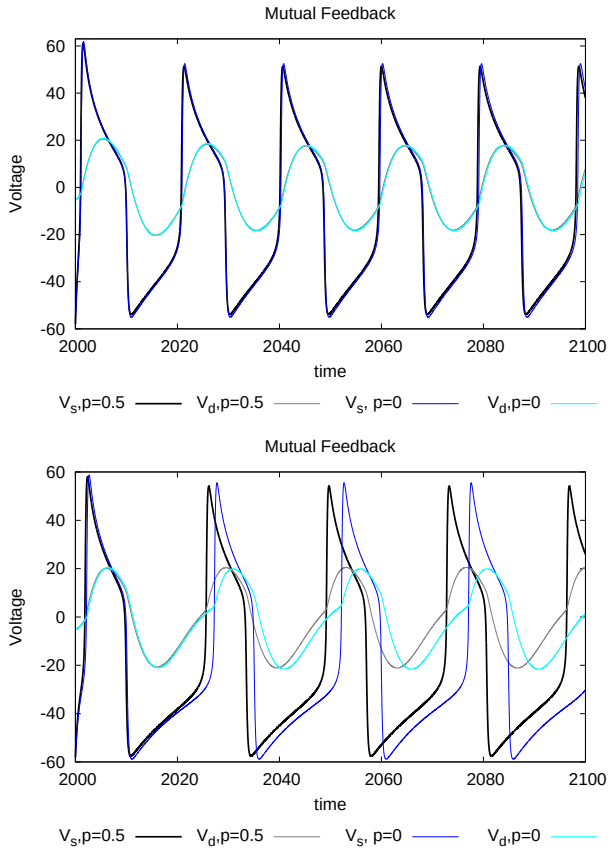

FIG. 8: Mutual feedback soma-dendrite for $R = 1$ $k\Omega$ and $L = 16.55$ kH such that $w^* = 0.25$ rad/ms. (Top) $I_s = 72$ μA gives $w_{soma} = 0.32$ $rad/ms > w^*$. (Bottom) $I_s = 50$ μA gives $w_{soma} = 0.25$ $rad/ms = w^*$. In black and gray the case when both directions are allowed, in blue and cyan the case when there is only current flowing from the soma into the dendrite.

As one can notice, firing at the natural frequency leads to an enhanced feedback on the soma. A larger amount of current flows back and therefore the soma itself feels an effective injected current greater than I_s, which makes it fire more frequently.

IV. SPATIALLY EXTENDED MODEL

In this section we introduce spatially extended dendrites. We model them as quasi-active finite cables through the following set of equations:

$$\begin{aligned} C\frac{\partial V_d(x,t)}{\partial t} &= -g_{L,d}V_d(x,t) + D\frac{\partial^2 V_d(x,t)}{\partial x^2}, \\ &\quad - I(x,t) + g_c(V_s(t) - V_d(x,t))\delta(x), \\ L\frac{dI(x,t)}{dt} &= -RI(x,t) + V_d(x,t), \end{aligned} \tag{16}$$

where $V_s(t)$ follows the set of equations (9). At $x = 0$ the dendrite is connected to the somatic compartment through g_c and at the other end of the cable we invoke the conservation of the current and therefore we fix

$$\left.\frac{\partial V_d(x,t)}{\partial x}\right|_{x=L} = 0. \tag{17}$$

According to Koch[11], the best way to study the resonant properties of a spatially extended dendrite is to take an infinitely-long cable and stimulate it using a delta spike $I_\delta = \delta(x - x_0)\delta(t - T)$ at the point x_0 and at time T. In the following we will then consider a very long dendrite weakly coupled with a non-firing soma and inject a delta stimulus far away from the origin. Recording the response of the dendrite at the distance Δx from the injection point and fixing R and L one gets the natural frequency $w^*(R, L; \Delta x)$ for that distance from the delta spike. In fig. **9** we show the response $V_d(\Delta x, t)$ of the dendrite for different distances Δx (top) and its (numerically computed) Fourier transform $\tilde{V}_d(\Delta x, w) = \mathcal{F}[V_d(\Delta x, t)]$ (bottom). The peak of the Fourier transform $\tilde{V}_d(\Delta x, w)$ correspond to the resonant frequency of the dendrite w^* at distance Δx and for fixed $R = 1$ $k\Omega$ and $L = 16.5$ kH. The observed values of the natural frequency are around the value obtained for the one compartment model $w^* = 0.25$ rad/ms, as expected. The values of the peaks are reported in fig. **10**, where we show the dependence of the resonant frequency on the distance Δx. Moreover, according to Koch[11], one can define

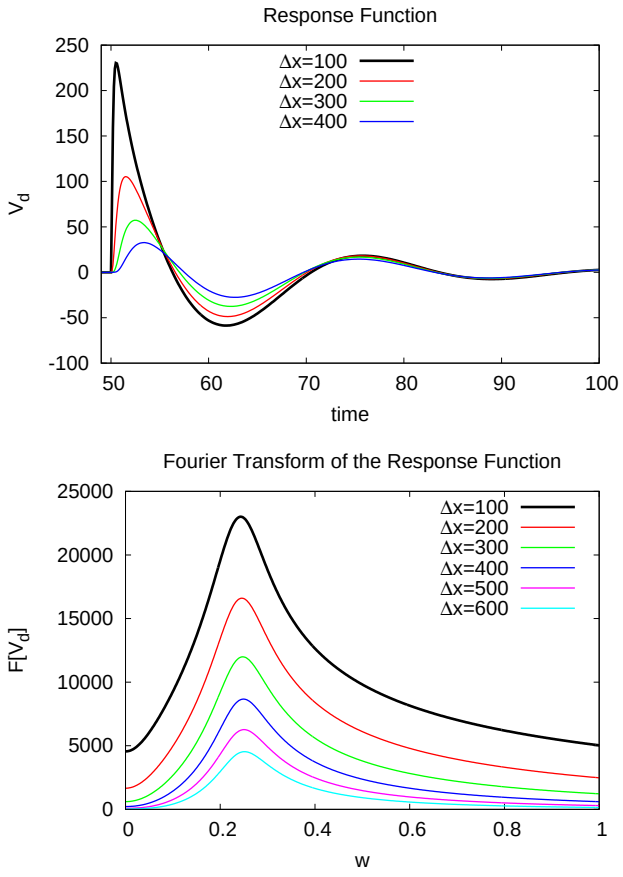

FIG. 9: (Top) Response function $V_d(\Delta x, t)$ and (Bottom) Fourier transform $\tilde{V}_d(\Delta x, w) = F[V_d(\Delta x, t)]$ for different distances $\Delta x[\mu m]$ from the injection point x_0. Here, the cable is long $L = 10^4\ \mu m$, $R = 1\ k\Omega$, $L = 16.5\ k\Omega$ and $D = 10^4\ \mu m^2/ms$.

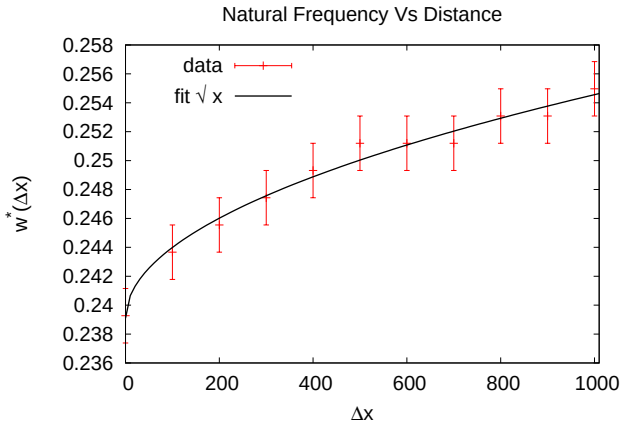

FIG. 10: Plot of $w^*[rad/ms]$ as a function of $\Delta x[\mu m]$. The frequency increases as the square root of the distance Δx.

the ratio between the amplitude of the response at the natural frequency $w = w^*$ divided by the amplitude of the response at $w = 0$, for fixed distance Δx:

$$q = \frac{|\tilde{V}_d(\Delta x, w^*(\Delta x))|}{|\tilde{V}_d(\Delta x, 0)|}, \tag{18}$$

which is a good measure of the quality of the band-pass filtering. In fig. **11** we show that q increases exponentially for increasing distances Δx, meaning that the further we record from the injection site the 'purer' the signal is.

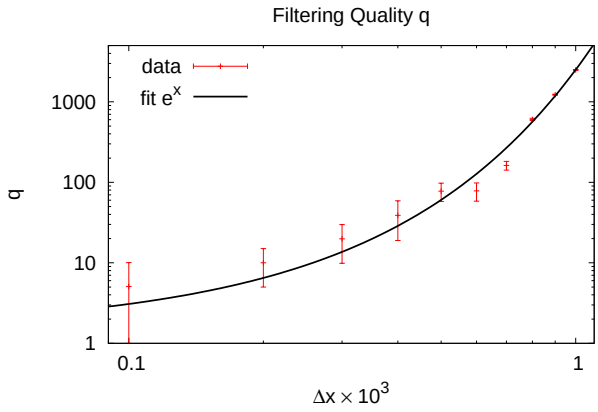

FIG. 11: Ratio q defined in (18) as a function of the distance $\Delta x[\mu m]$. Notice the exponential increasing of q meaning that all the frequencies $w \neq w^*$ are attenuated, and only $w \sim w^*$ can travel further along the dendrite.

In other words, the membrane filters the signal and allows only those frequencies close to the natural one to travel further along the cable. Even if the increasing of the band-pass quality is counterbalanced by the attenuation of the whole response function because of the leaking through the membrane, this is a remarkable result. This can, at least partially, explain the mechanism behind the tonotopical structure of the primary auditory neurons[1,2] where sounds with similar frequency are processed in topologically neighbouring regions in the brain, which means that neurons in the auditory cortex can be specialised in particular range of frequencies. The results shown above could even partially explain the ganglion cells differentiation in the retina[3,4] where visual stimuli with different temporal frequencies can be transmitted by different

type of cells, as for instance, parasol retinal ganglion cells which have been shown to respond best to high-temporal low-spatial frequency.

V. GREEN'S FUNCTION

As already mentioned in the introduction, we aim to describe networks of spatially extended neurons connected by gap-junctions. In the following we consider a small network made by two semi-infinite identical neurons joined at x_0 by a gap-junction g_J. From the numerical point of view Saraga and Skinner[10] have already shown the importance of the strength and location of the electrical junction between two dendrites. In particular, gap-junctions are responsible for complex dynamic patterns including antiphase or phase locking between the voltages in the joined dendrites. From an analytical point of view, Abbott *et al*[8] and then Coombes *et al.*[9] have suggested a possible approach at the level of single cell, using the sum-over-trips, or the path integral, method. This framework requires a form for the Green's function $G(x, y, t)$ which is made by a sum over all the possible trips that the signal experiences when travelling from a recording point x to an injection point y (in this framework the trips are constructed counter-intuitively from the recording point to the injection one) in the network. Even in the case of small networks, the reflections at the terminals and at the junctions make the sum running over an infinite number of terms. Here, we suggest a method to find an analytical compact form for the infinite sum of all the possible trips from x to y in the case of two semi-infinite identical neurons joined by a gap-junction. The equations governing the dendritic potential in the i-th branch are:

$$\begin{aligned} C\frac{\partial V_{d,i}(x,t)}{\partial t} &= -g_{L,d}V_{d,i}(x,t) + D\frac{\partial^2 V_{d,i}(x,t)}{\partial x^2} \\ &- I_i(x,t) + g_J(V_{d,j}(x,t) - V_{d,i}(x,t))\delta(x-x_0) \\ &+ I_{inj}(x,t), \\ L\frac{dI_i(x,t)}{dt} &= -RI_i(x,t) + V_{d,i}(x,t) \ , \end{aligned} \tag{19}$$

with $i = 1, 2$ and where this time we consider the somatic compartment as boundary condition

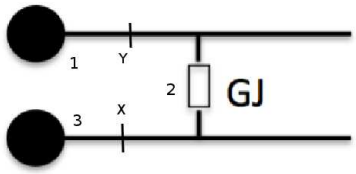

FIG. 12: Cartoon of our system in which is represented the gap junction connecting the dendrites i,j and the somatic compartments as boundary conditions for the semi-infinite dendrites. The numbers will be useful for our schematic approach later on.

for each dendritic cable and x_0 is the location of the gap-junction. In other words we impose $V_{d,i}(0,t) = V_{s,i}(t)$ at the finite end in both cells. Moreover, we need to impose the conservation of the current at $x = 0$ which can be written as:

$$C_s\frac{\partial V_{d,i}(0,t)}{\partial t} + g_s V_{d,i} - \frac{1}{r_a}\frac{\partial V_{d,i}(0,t)}{\partial x}\bigg|_{x=0} = 0 \tag{20}$$

where r_a is the axial resistance, C_s the capacitance and $g_{L,s}$ leakage conductance of the soma. At the other side of the cable we impose that $V_{d,i}(\infty, t) < \infty$. A cartoon of our system is shown in fig. **12**. Now, inspired by previous works on resonant dendrites[9], we will look for a compact form of the Green's function in the Laplace domain. As shown by Coombes *et al.*[9], it is very straightforward to work in the Laplace domain in the case of resonant dendrites, since the frequency dependence of the voltage is made explicit. If we Laplace transform a PDE of the following form (on an infinite domain):

$$\frac{\partial V(x,t)}{\partial t} - \frac{\partial^2 V(x,t)}{\partial x^2} = A(x,t), \tag{21}$$

we get:

$$(1 - d_{xx})\tilde{V}(x,w) = \tilde{A}(x,w). \tag{22}$$

Now using the definition of Green's function for generic operator $\hat{L}$:

$$\hat{L}G(x,y) = \delta(x-y), \tag{23}$$

we can solve equations of the form of eq. (22). In particular:

$$\hat{L}\tilde{V}(x,w) = \int_{-\infty}^{+\infty}\left[\hat{L}\tilde{G}(x,y,w)\right]\tilde{A}(y,w)dy, \tag{24}$$

and therefore, using the fact that $\hat{L} = 1 - d_{xx}$ is a linear operator acting only on x:

$$\tilde{V}(x,w) = \int_{-\infty}^{+\infty} \tilde{G}(x,y,w)\tilde{A}(y,w)dy, \quad (25)$$

which, in the case of eq. (19) and for vanishing initial conditions can be written as[9]:

$$\tilde{V}_{d,i}(x,w) = \int_{-\infty}^{+\infty} \tilde{G}_{ij}(x,y,w)\tilde{I}_{inj,j}(y,w)dy, \quad (26)$$

for injected current $\tilde{I}_{inj}(y,w)$ in the branch j at location y. Hence, if we know a form for $\tilde{G}(x,y,w)$ (we drop the indexes i,j since we have only two branches and the system is symmetric) then it is very likely to get the voltage response $\tilde{V}(x,w)$. Now, in order to get a form for the Green's function in the case of our toy model depicted in fig. **12**, we can use two major results. First, the fact that the Green's function for an infinitely long cable takes the form[9]

$$\tilde{G}_{\infty}(x,y,w) = \frac{e^{\gamma_D(w)|x-y|}}{2\gamma_D(w)D}, \quad (27)$$

with

$$\gamma_D^2(w) = \frac{1}{D}\left[\frac{g_{L,d}}{C} + w + \frac{1}{C}\frac{1}{R+wL}\right]. \quad (28)$$

Second, the fact that in the case of complicated branching structures the total Green's function can be simply written as[8,9]

$$\tilde{G}(x,y,w) = \sum_{trips} A_{trip}(w)\tilde{G}_{\infty}(L_{trip},w). \quad (29)$$

where $A_{trip}(w)$ takes into account the coefficients at the nodes and at the terminals when the signal is reflected or passes through them. In the following section we will derive a form for A_{trip} using a simple method that associates at each possible trip a unique word.

A. Method of Words

In the following we derive a compact form for all the possible trips which can be chosen by the signal using 'words'. Each word (or trip) is made by 'letters' which can combined. We then fix the rules governing the assembling of the letters such that we restrict our dictionary (or set of words) to only those which are allowed in our system. Finally we associate at each pair of letters (syllable) a value which correspond to the coefficients given in literature[9] for the transmission or reflection of the signal when interacting with a node or a terminal.

1. Alphabet

We can notice that the useful trips are only those which do not get lost at infinity. Therefore, we can consider the subsystem enumerated with the numbers in fig. **12**. This system is a graph with three nodes (two end points where the soma are placed (namely '1' and '3') and one where the dendrites interact (namely '2')) and two points (say x and y) on the dendrites. Our alphabet consists of 4 letters:

$$2 \to 1 \equiv A$$
$$1 \to 2 \equiv B$$
$$2 \to 3 \equiv Y$$
$$3 \to 2 \equiv Z$$

2. Rules

The rules that we impose for our system are the following:

- Every word must start with B or AB;
- Every word must finish with Y or YZ;
- Every time an A occurs must be always followed by a B;
- If Y is not the end of the word, it can be followed only by Z;
- If Z is not the end of the word, it can be followed only by the pair AB or Y;

with these rules we can form the words of our vocabulary. In particular, our rules tell us explicitly that the most minimal word is BY followed by ABY and BYZ which are followed

by $ABYZ$, and so on. Our goal is to take advantage of the rules such that they lead us toward the solution.

3. Meanings

Now we have to associate the syllables with a meaning, or a value. Below we use the coefficients given in literature[9] for signals reflecting at a soma $(2p_s - 1)$ and for signals passing through or reflecting $(\pm p_g)$ at the gap-junction.

	A	B	Y	Z
A	0	$2p_s - 1$	0	0
B	$-p_g$	0	p_g	0
Y	0	0	0	$2p_s - 1$
Z	p_g	0	$-p_g$	0

These coefficients are obtained imposing current conservation at the nodes and we refer to the literature for the complete derivation of them[9]. They take the forms

$$p_g(w) = \frac{1}{2z(w)/g_J + 1} \tag{30}$$

$$p_s(w) = \frac{z(w)}{z(w) + \gamma_S(w)} \tag{31}$$

where $z(w) = \gamma_D(w)/r_a$ is the impedance of the cables and $\gamma_S(w) = C_s w + g_{L,s}$.

For the purposes of this section they are only values to be given at each syllable. Notice that we have to give a value to each syllable in the word, for instance the word $ABYZ$ has 3 syllables which are AB, BY and YZ.

4. Examples

Let us, for instance, build the shortest trips of the voltage in our system. We therefore look for the minimal words of our dictionary. Given our rules, the most sensible choices are

$$BY + BYZ + ABY + ABYZ, \tag{32}$$

which can be rearranged in a compact form:

$$(1 + A)BY(1 + Z). \tag{33}$$

In this compact form we loosely use the symbol 1 with the meaning 'no letters'. The word: $1BY1$ is therefore BY. The expression (32) has meaning (reading all the syllables):

$$p_g + (2p_s - 1)p_g + p_g(2p_s - 1) + (2p_s - 1)p_g(2p_s - 1) \tag{34}$$

which has an equivalent compact form

$$[1 + (2p_s - 1)]\, p_g\, [1 + (2p_s - 1)] \tag{35}$$

or, in the language of trips:

$$\begin{aligned} &\{y \to 2 \to x\} \\ &\{y \to 1 \to y \to 2 \to x\} \\ &\{y \to 2 \to x \to 3 \to x\} \\ &\{y \to 1 \to y \to 2 \to x \to 3 \to x\} \end{aligned}$$

It is worth noting that these are the four shortest trips, and therefore they are the the most important terms in $A_{trip}(w)$.

5. Longer Paths, Longer Words

Obviously, longer trips are associated to longer words. But, at the same time, we have already obtained a skeleton for all our words. In fact, we can generate an infinite number of words following the rules, but they all must start with B or AB and finish with Y or YZ. The trick we use is to keep the 'skeleton' (33) and generate as many copies of the words AB and YZ as we want inside of it. The best way to do this is using the combinatorics. In fact, using the symmetry of the system we know that the order of the syllables do not count. For instance, a section of a trip that looks like $ABYZ$ has the same coefficients of $YZAB$ and therefore we will simply count twice $ABYZ$. The only subtlety to take into account is the sign of the term, which gets a minus sign if the path is reflected an odd number of times at '2'. The suggested form for the 'body' is:

$$\sum_{n=0}^{\infty} \sum_{k=0}^{n} \binom{n}{k} (-1)^n (AB)^k (YZ)^{n-k}. \tag{36}$$

Now, taking into account that

$$AB^k = YZ^k = (2p_s - 1)^k p_g^{k-1}$$

we assign to (36) the meaning

$$\sum_{n=0}^{\infty}\sum_{k=0}^{n}\binom{n}{k}(-1)^n(2p_s-1)^k p_g^{k-1}p_g \\ (2p_s-1)^{n-k}p_g^{n-(k-1)}, \tag{37}$$

and hence (using $\sum_{k=0}^{n}\binom{n}{k}=2^n$):

$$\sum_{n=0}^{\infty}\sum_{k=0}^{n}\binom{n}{k}(-1)^n p_g^{n+1}(2p_s-1)^n = \sum_{n=0}^{\infty}\left[-2p_g(2p_s-1)\right]^n p_g. \tag{38}$$

In particular, one can convince himself that the trips are labelled by n such that $n+1$ is the number of reflections plus the number of passings through the gap-junction. We now can consider the 'skeleton' (33), taking care to do not count p_g twice. But first, we focus on the length of the trips.

B. Length of the Trips

Until now we did not consider the difference in length of the trips. Since the general form for the Green's function $G(x,y,w)$ is

$$G(x,y,w)=\sum_{trips}A_{trip}(w)G_\infty(L_{trip},w) \tag{39}$$

we need to take into account the length of each trip generated by (38)+'skeleton'. From now on, we set the the origin at the gap-junction, and both the somatic compartments at L. We recall that the current is injected at y and measured at x. With this choice of the axes, the distance from the points x and y to the somatic compartments on the respective branches are respectively $L-x$ and $L-y$. Moreover, with this convention, the shortest trip has length $y+x$. The one that reflects into the first soma has length $2L+(x-y)$ while the trip that reflects into the second soma has length $2L+(y-x)$. Finally the fourth shortest trip which reflects to into both somatic compartments has length $4L-(y+x)$. We can generalise this procedure for any trip and in particular we can simply assign different length to the four different classes of trips mentioned above and represented by the only 'skeleton'. In other words, we can keep (38) as it is and write (39) as:

$$\begin{aligned}G(x,y,w)=&\sum_{n=0}^{\infty}\left[-2p_g(2p_s-1)\right]^n p_g\times\\ &\times\{G_\infty(2nL+(y+x),w)+\\ &+(2p_s-1)G_\infty(2(n+1)L+(x-y),w)+\\ &+(2p_s-1)G_\infty(2(n+1)L+(y-x),w)+\\ &+(2p_s-1)^2G_\infty(2(n+2)L-(y+x),w)\}\end{aligned} \tag{40}$$

C. Numerical Validation

In this section we want to validate our theoretical Green function in the Laplace domain comparing it with the results from brute force simulations. We decide to consider for the moment passive dendrites ($R\to\infty$) and then generalise our results to quasi-active ones in a second step. Since in our simulations we can record $V_d(x,t)$, we need to inject a delta spike such that the Green's function $G(x,y,t)$ coincide with the potential at x. Moreover, in order to compare our results we need first to take the inverse Laplace transform of (40), such that theoretical curve and numerical data can be compared in the time domain. By looking at (40), it is clear that the analytical inversion could be a very difficult task therefore we choose to invert it using a numerical procedure. The strategy adopted involves the so called Bromwhich integral, defined as:

$$F(t)=\frac{1}{2\pi i}\int_{\Gamma-i\infty}^{\Gamma+i\infty}e^{st}f(s)ds \tag{41}$$

where Γ is a real value which defines a vertical contour in the complex plane and must be chosen such that the all the singularities of $f(s)$ are to the left of it. Using the fact that the only poles of our integrand are given by $G_\infty(x,w)$ which is of the form

$$G_\infty(x,w)=\frac{e^{-\gamma_D(w)|x|}}{2\gamma_D(w)D} \tag{42}$$

with $\gamma_D(w) = \sqrt{(w + g_{L,d}/C)/D}$ for passive dendrites. Therefore our only pole is on the negative part of the real axis and hence we can choose $\Gamma = 0$. Now eq. (41) can be written as a Fourier transform simply substituting $s = iw$

$$F(t) = \frac{1}{2\pi} \int_{-\infty}^{\infty} e^{iwt} f(iw) dw \qquad (43)$$

which gives the Fourier transform of the function $f(iw)$. We can therefore take the numerical inverse Fourier transform $\mathcal{F}^{-1}[G(x, y, iw)]$ to obtain $G(x, y, t)$.

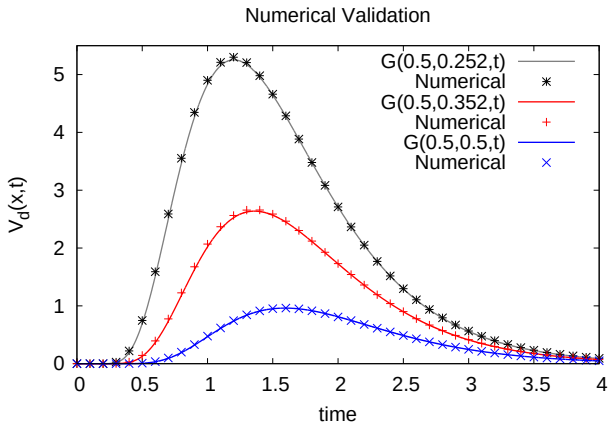

FIG. 13: Response function $G(x, y, t) = V_d(x, t)[mV]$ for a delta stimulus injected at y. The recording point is fixed at $x = 0.5$. The injecting sites are at $y = 0.252$, $y = 0.352$ and $y = 0.5$.

The curves in fig. **13** are given by method explained above, while the points are given by the brute force numerical simulations. The matching is remarkable, meaning we found a compact form for $G(x, y, w)$ which can be used more generally for resonant dendrites. Moreover, would be of great interest to compare numerical results obtained by Skinner *et al.*[10] with our analytical results.

VI. CONCLUSIONS

In this paper we reviewed the linearised model for active-membranes and studied numerically their band-pass properties in the case of point-like and spatially extended dendrites. We analytically found an expression for the complex impedance $Z(R, L)$ for the dendritic compartment and studied how the strength of the connection between somatic and dendritic compartments affects the dynamics of the voltage and the dendritic impedance. We also demonstrated how the resonant properties of the system alter the mutual feedback between the compartments. In particular, we showed that the closer the soma's firing frequency to the dendritic resonant one w^*, the higher the effective current in the somatic compartment is, and therefore the faster the soma fires. In the case of the spatially extended model, we introduced the function q as index of the quality of the band-pass filtering. We observed that the further we record from the injecting point along the same dendrite, the better filtered the signal is. This means that the combination of activity and spatial extension gives rise to stunning dendritic frequency selection. As we stated in the paper, this amazing property could explain many biologically observed features, as cortical neurons sounds selection and changing in dimension of the receptive field in the retina.

We then studied the role of the gap-junction at the network level. We suggested a compact analytical form for the Green's function in the Laplace domain in the case of a small network of semi-infinite quasi-active dendrites joined by a gap-junction. Even if we validated our analytically found Green's function only for the case of purely passive dendrites, our formalism also support the resonant membranes. A more difficult but more interesting task would be the extension of the language method explained in the paper to the case of more realistic geometries with finitely-long dendrites, as in the case of starbust amacrine cells. In this case much more reflections have to be taken into account. On the other hand, we hope that for symmetric geometries the language method will still be useful to find compact forms for $G_{ij}(x, y, w)$. Finally, we would like to explore the role of the gap-junction, especially from an analytical point of view. In particular, would be interesting to to compare the analytical results given by the Laplace transform $\mathcal{L}^{-1}[G_{ij}(x, y, w)]$ obtained varying the location and the strength of the gap-junction, with the numerical results given by Saraga *et al.*[10].

Acknowledgements

The authors are thankful for funding by the EPSRC.

Appendix A: Morris Lecar Parameters

The parameters for the Morris-Lecar model are:

V_1	=	-1.2 mV
V_2	=	18 mV
V_3	=	12 mV
V_4	=	17.4 mV
V_{Ca}	=	120 mV
V_K	=	-80 mV
V_L	=	-60 mV
g_{Ca}	=	4.0 mS
g_K	=	8 mS
g_L	=	2 mS
ϕ	=	1/15 ms^{-1}
C	=	1.0 μF

The (lower) Hopf bifurcation in the standard model occurs for values of the external current $i_s \sim 40\mu A$. This choice of the parameters leads to a type II neuron, namely, we observe a discontinuous transition between stable point and stable limit cycle[12].

Appendix B: Units of measurement

In this paper the units of measure are completely arbitrary. The standard biologically inspired units are ms for time, μm for space, mV for voltage, μA for current, $k\Omega$ for resistance, $kH = k\Omega/s$ for inductance and μF for capacitance. We could have chosen different units of measure and everything would be still valid. Therefore throughout this paper we will use the biologically inspired convention even though it is often useful to bear in mind that we give more general results.

Appendix C: Somatic Firing Frequency

In this section we report a table and a plot of some of the values of w_{soma} as a function of the injected current I_s directly measured from the plotted voltage dynamics of an isolated soma.

i_s $[\mu A]$	w_{soma} [rad ms^{-1}]
50	0.252
60	0.294
70	0.319
75	0.329
80	0.337
85	0.342
100	0.349

FIG. 14: Table with some values of w_{soma} as a function of I_s directly measured.

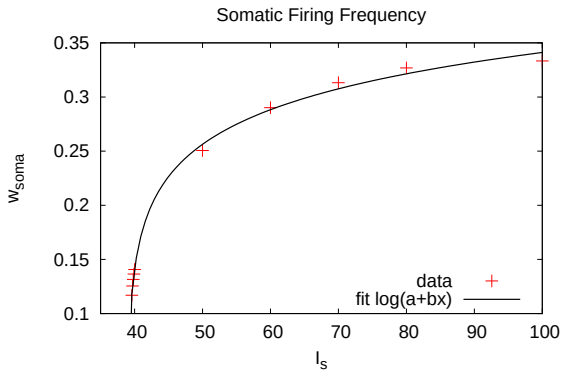

FIG. 15: Soma's firing frequency w_{soma} $[rad/ms]$ as a function of input current $I_s[\mu A]$. The data have been obtained measuring the period of the oscillations of a Morris-Lecar isolated model.

[1] Crawford, Fettiplace, *The frequency selectivity of auditory nerve fibres and hair cells in the cochlea of a turtle*, J. Physiol. 306, 79-125 (1980)

[2] M.P. Kilgard, M.M. Merzenich, *Order-sensitive plasticity in adult primary auditory cortex*, PNAS **99**, 3205-3209 (2002)

[3] Torre, Owen, *High-pass filtering of small signals by the rod network in the retina of the toad*, Biophys. J. 41, 305-324 (1983)

[4] Boycott, Wassle, *The morphological types of ganglion cells of the domestic cat's retina*, J. Physiol. **240**, 397-419 (1974)

[5] S.A. Burns, A.E. Elsner, *Response of the retina at low temporal frequencies* J. Opt. Soc. Am. **13**, 3 (1996)

[6] A. Mauro, F. Conti, F. Dodge, R. Schor, *Subthreshold Behaviour and Phenomenological Impedance of the Squid Giant Axon*, Journal of General Physiology **55**, 497-523 (1970)

[7] C. Koch, T. Poggio, *A simple algorithm for solving the cable equation in dendritic trees of arbitrary geometry*, Journal of Neuroscience Methods **12**, 303-315 (1985)

[8] Abbott, Fahri, Gutmann, *The path integral for dendritic trees*, Biol Cybern 66, 49-60 (1991)

[9] S. Coombes, Y. Timofeeva, C.-M. Svensson, G.J. Lord, K. Josić, S.J. Cox, C.M. Colbert *Branching dendrites with resonant membrane: a 'sum-over-trips' approach* Biol. Cybern. **97**, 137-149 (2007)

[10] F. Saraga, L. Ng, F. Skinner, *Distal Gap Junction and Active Dendrites can Tune Network Dynamics* J. Neurophysiology **95**, 1669-1682 (2006)

[11] C. Koch, *Cable Theory in Neurons with Active, Linearised Membranes* Biol. Cybern. **50**, 15-33 (1984)

[12] C. Morris, H. Lecar, *Voltage Oscillations in the Barnacle Giant Muscle Fiber*, Biophys. J., **35**, 192-213 (1981)